We are IntechOpen, the world's leading publisher of Open Access books Built by scientists, for scientists

4,800
Open access books available

122,000
International authors and editors

135M
Downloads

Our authors are among the

154
Countries delivered to

TOP 1%
most cited scientists

12.2%
Contributors from top 500 universities

CLARIVATE ANALYTICS BOOK CITATION INDEX INDEXED

WEB OF SCIENCE™

Selection of our books indexed in the Book Citation Index in Web of Science™ Core Collection (BKCI)

Interested in publishing with us?
Contact book.department@intechopen.com

Numbers displayed above are based on latest data collected.
For more information visit www.intechopen.com

12

Sinterability and Dielectric Properties of $ZnNb_2O_6$ – Glass Ceramic Composites

Manoj Raama Varma, C. P. Reshmi and P. Neenu Lekshmi
Materials and Minerals Division,
National Institute for Interdisciplinary Science and Technology
[NIIST],Thiruvananthapuram,
India

1. Introduction

In the new era of communication technology there are revolutionary developments in satellite communication, global positioning systems and mobile communication systems, which has helped the developments in multilayer technologies like low temperature cofired ceramics (LTCC). The microwave electronic devices have achieved significant miniaturisation, light weight and became very cost effective using LTCC. The characteristic properties required for dielectric materials which are used in multilayers are (a) high dielectric permittivity(ε_r), (b) high quality factor (Q×f) and (c) low temperature coefficient of resonant frequency (τ_f). The size of the resonator is inversely related to the $\sqrt{\varepsilon_r}$. Dielectric materials should posses near zero temperature coefficient of resonant frequency (τ_f) for thermally stable electronic devices [1-7].

Generally most of the dielectric ceramic materials are known to posses the above said properties but will sinter at temperatures above 1000 ^oC. Zinc niobates, $ZnNb_2O_6$ (ZN) is a low loss dielectric material with columbite structure having excellent dielectric permittivity, high quality factor and low temperature coefficient of resonant frequency. Sintering temperature of ZN is comparatively lower (~1200 ^oC) [8]. Hence it is widely used as dielectric resonators in microwave communication devices. In multilayer ceramic structures, the low melting electrodes such as Ag (melting point ~961 ^oC), Cu (melting point ~1083 ^oC) and Au (melting point ~1064 ^oC) are co-fired with these ceramic materials [9,10]. In the case of Ag electrodes, processing temperature of the material must be below 950 ^oC.

There are several approaches to reduce the sintering temperature of the ceramics viz. (i) usage of ultra-fine particles/powders as synthesized by wet chemical methods as starting materials (ii) addition of low melting glasses to obtain a low temperature sintering composite [11-14]. Glass addition is known to be the most popular and least expensive method and hence ZN is widely used in ceramic technology.

Even though the ZN ceramics prepared by conventional ceramic route [1-6] shows excellent properties, high sintering temperature preclude its application potential in the LTCC. Usage of nano sized ZN powders (instead of micron size powders) in multi layer technology can bring down the sintering temperature to a lower value. Hence the procedure for preparing

ZN ceramic powder as both micron size powders and nanosized powders and the sinterability of pure materials as well as the glass added ceramics are described in this chapter. The structural characterisation of the materials can be done using XRD and the microwave dielectric properties (in the frequency range 2-6 GHz) can be studied and compared to highlight the effect of particle size on sinterability and microwave dielectric properties of these materials.

2. Materials and methodologies

ZN ceramic powders can be synthesized using two different well established preparation techniques such as solid state ceramic method and polymer complex techniques [15-17].

2.1 Synthesis of $ZnNb_2O_6$ using solid state synthesis technique

Single phase ZN can be prepared using oxides of Zn (ZnO 99.9+%) and pentoxide of Niobium (Nb_2O_5 99.9+%) as raw materials. These oxides can be weighed in stoichiometric proportion and mixed for 24h in a ball mill, using zirconia balls and distilled water as the milling medium. The slurry can be dried at 80 ^oC and the dried powder can be calcined at 850 ^oC/4h, to get the phase pure ZN ceramics.

2.2 Preparation of $ZnNb_2O_6$ using polymer complex method

Zinc acetate [$Zn(CH_3COO)_2$ 99.99%,] and niobium ethoxide [$Nb(OC_2H_5)_5$, 99.95% metal basis] can be used as the starting material for preparing ZN using polymer complex method. The flow chart, in Fig. 1 shows the various steps involved in the synthesis. 3 mol equivalent of citric acid can be dissolved in 12 mol of ethylene glycol with continuous stirring for 1h to form a clear solution. 1 mol of zinc acetate can then be added and stirred for several hours at 80^oC to dissolve it completely. 2 mol of $Nb(OC_2H_5)_5$ can be added to this clear solution with a stirring speed of 500 rpm until it results in the formation of a thick white gel. The gel can be sonicated for 2h to obtain the uniform distribution. After sonication the polymeric precursor can be recovered by desalting with acetone. The dried polymeric precursor can be calcined at 600^oC/4h to obtain the $ZnNb_2O_6$ nanopowders.

2.3 Preparation of $60ZnO\text{-}30B_2O_3\text{-}10SiO_2$ (ZBS) glass

High purity ZnO, B_2O_3 and SiO_2 (99.9%) can be used as the raw materials for the preparation of $60ZnO\text{-}30B_2O_3\text{-}10SiO_2$ (ZBS, sintering temperature is <800 ^oC). The raw materials weighed accurately in the stoichiometric proportion are mixed well in distilled water medium using zirconia balls for 24 h in a ball mill. The slurry can be dried and the powder can be melted in a platinum crucible at 1000^oC for 2h, and the melt can be quenched into cold distilled water and powdered. This glass powder can be used for the preparation of glass ceramic composites.

2.4 Preparation of ZN-ZBS glass composites

Appropriate amounts of ZN and ZBS glass (1,3,5,10 wt%) can be mixed using an agate mortar for 2 hours in distilled water medium and the slurry can be dried and powdered. 3wt% PVA solution can then be added to this mixture as a binder. The dried powder can be uniaxially pressed using a tungsten carbide (WC) die in the form of cylindrical discs of

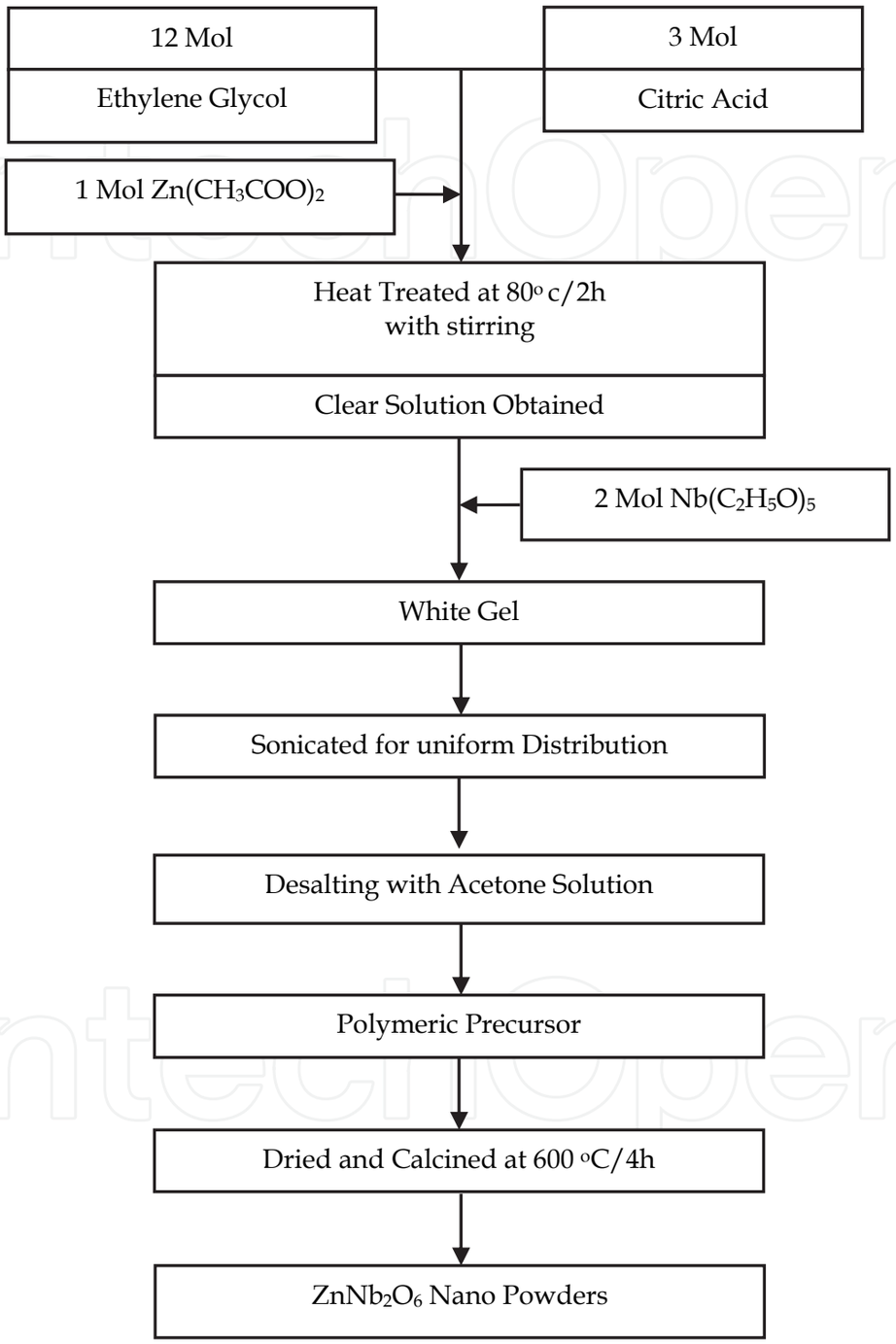

Fig. 1. Flow chart for the preparation of $ZnNb_2O_6$ nano powders

diameter 14 mm and about 7 mm height at a pressure of 150 MPa. The green compact can be heat treated at different temperatures and the dimension changes are recorded. The density can be determined each time and the sintering temperature can be optimised as the temperature which gives the maximum densification.

The sintered pellets of all the compositions can powdered and the crystalline phase of the powders are identified by the XRD analysis using Cu-Kα radiation of wavelength (λ) 1.54056Å for 2θ range 10-80^{o}. The recorded patterns are compared with standard ICDD Data file with the help of Philips X'pert High Score plus software. The ZN nano particles can be characterised using transmission electron microscopy (HRTEM) FEI Technai G^2 30S-TWIN high resolution electron microscope operated at 300 KV. The crystallite size, lattice parameter and the selected area diffraction patterns can be recorded using TEM. The crystallite size (d) of the nano-ZN was determined from the XRD patterns using Debye Sherrer formula [18,19],

$$d = \frac{0.9\lambda}{\beta \cos\theta} \tag{1}$$

where λ is the wavelength of the x-ray, β is the FWHM of the maximum intense peak and θ is the glancing angle.

The microstructure analysis of the sintered polished and thermally etched samples can be carried out using scanning electron microscope (SEM, JEOL-JSM, 5600LV, Tokyo, Japan). The bulk densities of the sintered pellets can be measured by the Archimedes method. The dielectric constant can be measured using the post resonator method of Hakki and Coleman modified by Courtney. The unloaded quality factor can be measured by a resonant copper cavity whose interiors are coated silver and the ceramic composites are placed on a low loss quartz spacer which reduces the effect of losses due to surface resistance of the cavity using a Vector Network Analyser. The temperature coefficient of resonant frequency (τ_f) can be measured by noting the temperature variation of the same using $TE_{01\delta}$ mode in the transmission configuration over a range of temperature 20-80^{o}C. The temperature coefficient of the resonant frequency can be calculated using the following relation in a fixed interval of temperature [20-22],

$$\tau_f = \frac{f_2 - f_1}{f_1 (T_2 - T_1)} \tag{2}$$

where, f_1 and f_2 are the resonant frequencies at temperatures T_1 and T_2 respectively and the average value can be calculated and reported.

3. Observations and analysis

Fig 2(a) is the powder XRD diffraction pattern of $ZnNb_2O_6$ synthesized using solid state ceramic route. All the peaks are compared with the ICDD file card for ZN (Number 76-1827) and indexed. Fig 2 (b) depicts the XRD pattern of $ZnNb_2O_6$ with 5wt% of zinc borosilicate glass (ZBS). The addition of ZBS glass did not produce any additional phases, as evident from Fig. 2 (b).

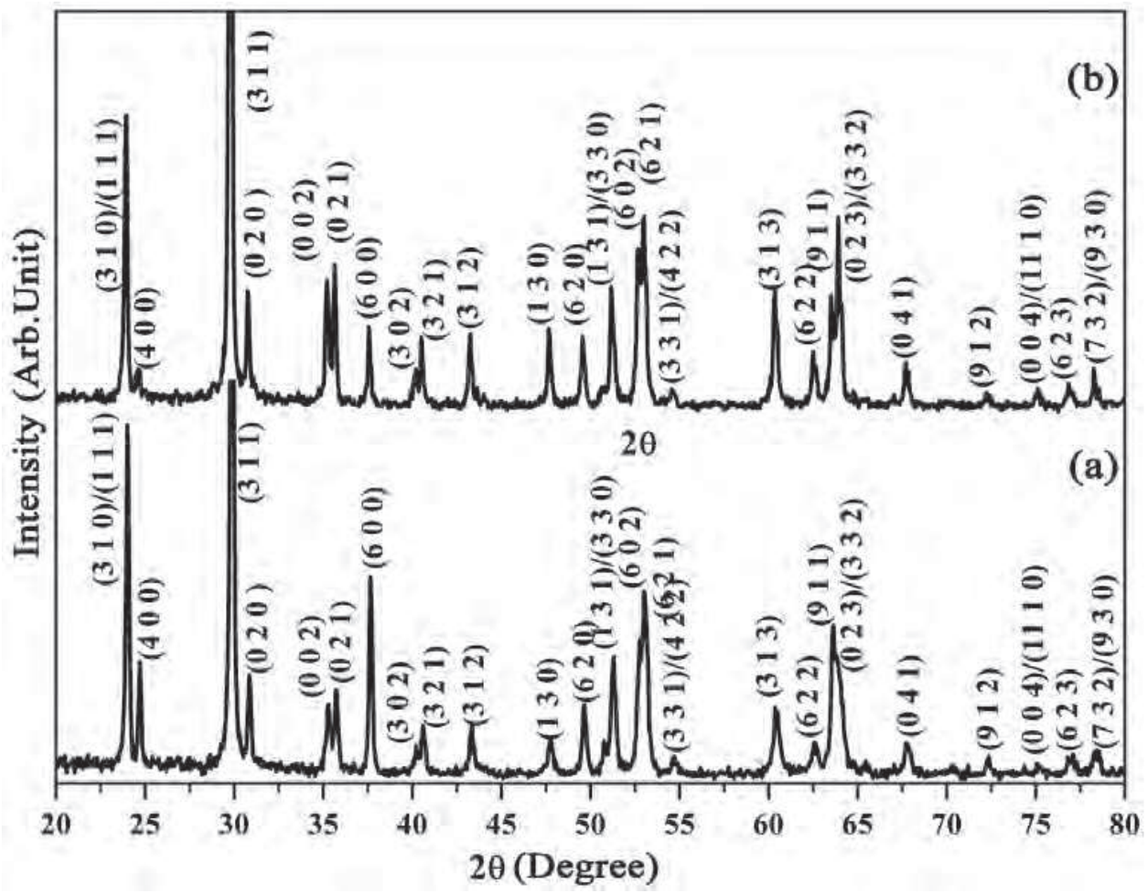

Fig. 2. XRD pattern of $ZnNb_2O_6$ (a) sintered at 1200°C/2h and (b) $ZnNb_2O_6$ + 5Wt%

The powder XRD patterns of the calcined $ZnNb_2O_6$ nanopowders are depicted in the fig 3. Fig 3(a) shows the XRD pattern of $ZnNb_2O_6$ calcined at 600°C/4h and fig 3 (b) is that of $ZnNb_2O_6$ powder sintered at 950 °C/2h. The figures clearly indicate that the powder patterns are in well accordance with ICDD data card (76-1827). The average crystallite size of the nanostructured ZN calcined at 600 °C/4h can be estimeted from the X-ray diffraction pattern. The fig 4 depicts the maximum intense peak obtained from XRD of ZN ceramics. Using Gaussian fit (as seen in the fig 4), the FWHM and centre of the peak can be determined. Employing Debye Sherrer formula (equation 1) the average crystallite size can be calculated as ~17 nm.

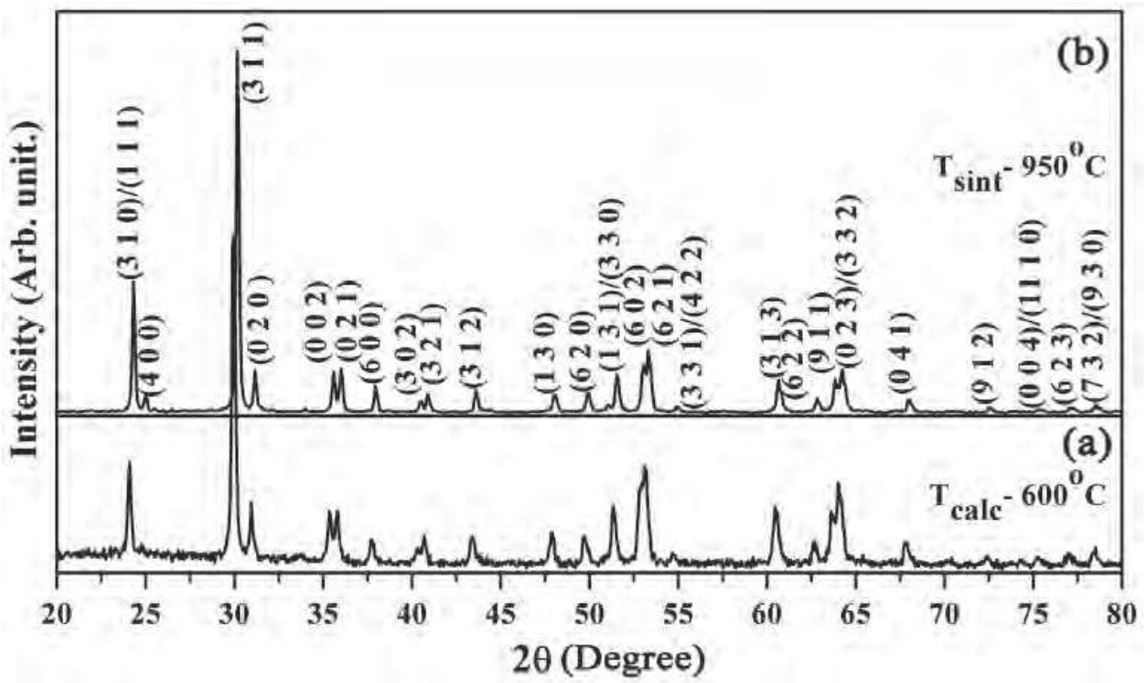

Fig. 3. XRD pattern of $ZnNb_2O_6$ (a) calcined at 600°C/4h and (b) calcined at 950°C/2h.

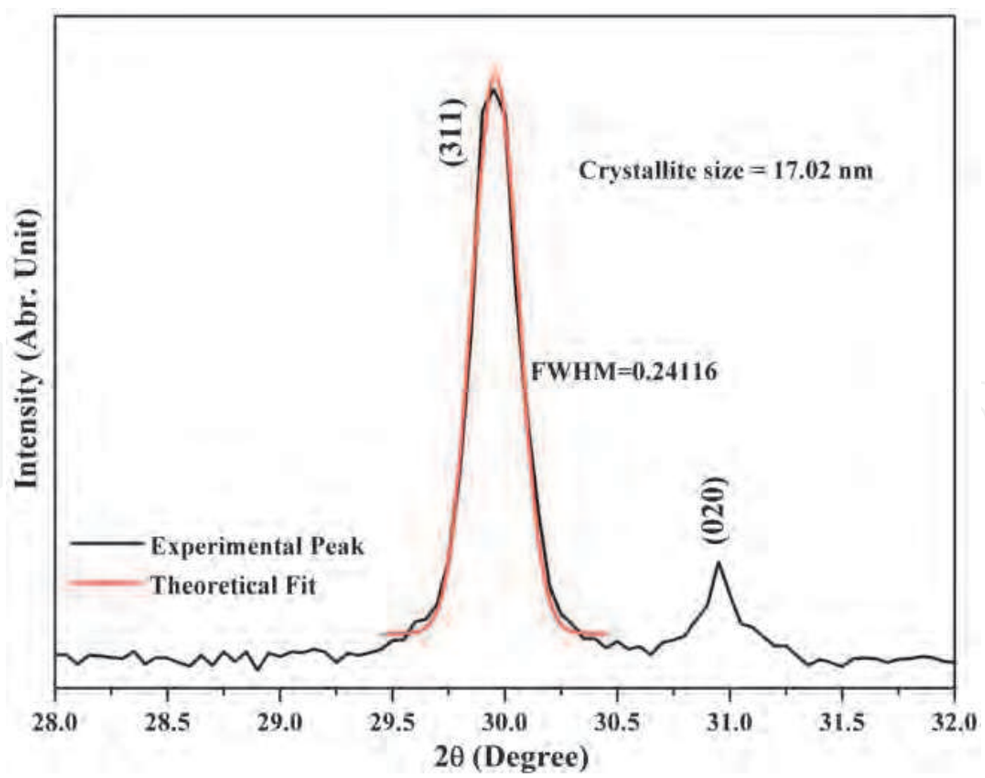

Fig. 4. Maximum intense peak in XRD pattern of nanostructured ZN ceramics with theoretical Gaussian Fit

Fig 4 shows the various TEM images of ZN nanocrystallites. Fig 5 (a), (b) and (c) are the TEM images of the ZN nanocrystallites at two different regions. It can be seen that in both images the nanocrystallites have same characteristics and mostly of spherical in shape. The fig 5 (c) establishes the crystallite size at low magnification; they are well separated and have uniform size distribution. A histogram is shown in fig 5 (d), indicates the crystallite size obtained from the images both fig 5 (a) and (b). In order to obtain particle size distribution, a Gaussian function is fitted for the experimental data. The average particle size is obtained and found that it is lies between 18-20 nm. This is in good agreement with the crystallite size obtained from XRD using Debye Scherrer formula.

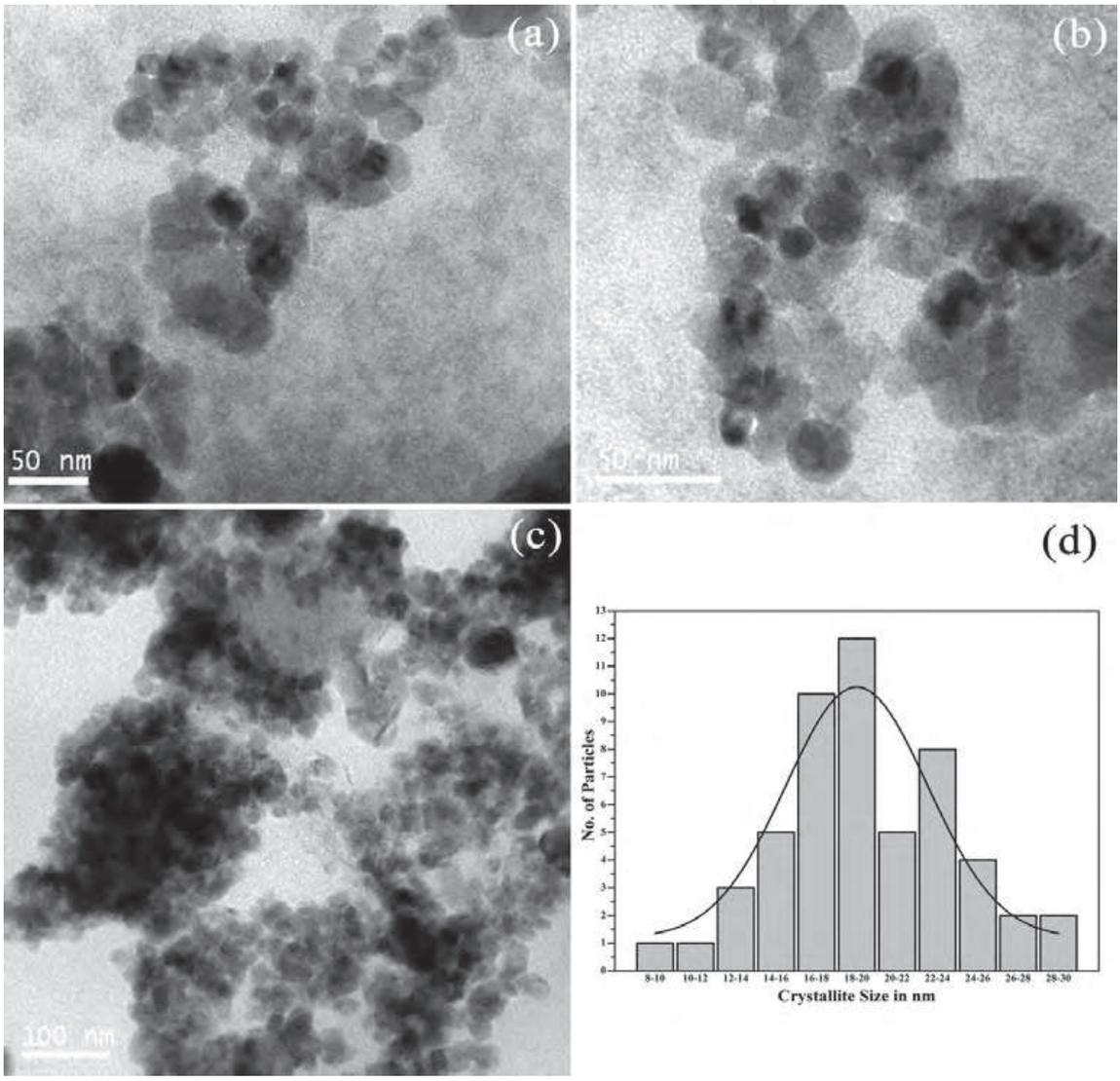

Fig. 5. TEM images of nano $ZnNb_2O_6$ (a), (b) 50 nm scale, (c) 100 nm scale and (d) histograph of particle size distribution obtained from image (a) and (b).

The high resolution TEM (HRTEM) image and the selected area diffraction pattern (SADP) of ZN nanocrystallites are shown in the fig 6 (a) and (b) respectively. Lattice plane of ZN nanoparticles are clearly visible in the HRTEM image. Inter planar spacing 'd' of several planes were determined using set of Fourier Transforms of lattice fringe images. TEM image analysis software (Digital Micrograph - Gatan) was used for the determination of interplanar spacing. The average d values were determined and the plane corresponding to each set of fringes are duly indexed, shown in the fig 6 (a). Interplanar spacing obtained from TEM and XRD are tabulated in table 2. Comparing the d values from the X-ray diffraction pattern, the planes corresponding to each ring was identified and indexed.

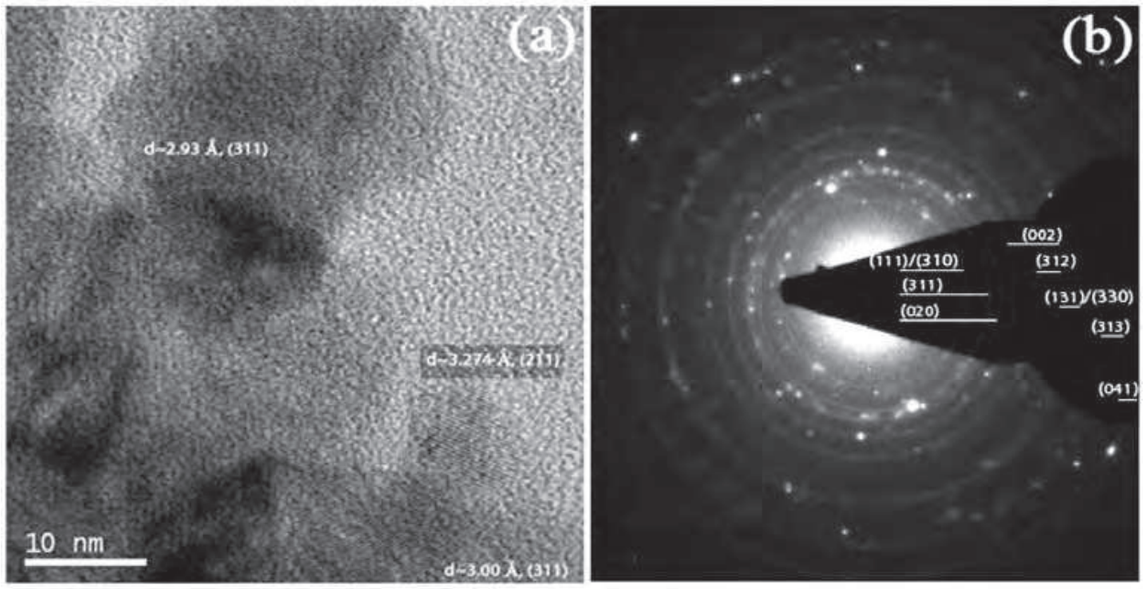

Fig. 6. (a) HRTEM of nanostructured ZN ceramic (b) SAD patterns of ZN ceramics.

In fig 7, variation of bulk density of pellets, synthesised by solid state ceramic route and heat treated at 975°C with different wt% of ZBS is shown. From the fig 7, ZN ceramics with 5 wt% of ZBS has maximum density. Hence 5 wt% of ZBS is taken as the optimized glass addition amount for the composite. Fig 8 illustrates the variation of the bulk density of ZN and ZN-ZBS glass composites with varying sintering temperatures. From Fig. 8 it can be seen that nanostructured ZN with 5 wt% of ZBS glass has greater density at lower sintering temperatures (925°C/2h). Comparison of densification of pure (nano and micron sized) ZN ceramics shows that the densification is faster for nano powder compacts at lower temperatures, however at temperature above 1100°C for micron sized powder compacts synthesised by solid state ceramic route has higher absolute density. Since the nano powders of ZN have higher sinterability, the growth during the sintering process will be more rapid. Hence more finer intergranular porosities will be formed in the case of nano powder compacts than micron sized powder compacts. This will results in the reduction in the values of absolute densities of sintered powder compacts. Similar effects were noticed for sintered nano sized powder compacts of BZT by Manoj Raama Varma et al. [23] In nanostructured ZN ceramics the grain boundary area per unit volume will be more than that of the solid state synthesised ZN ceramics [24]. This deteriorates the densification of

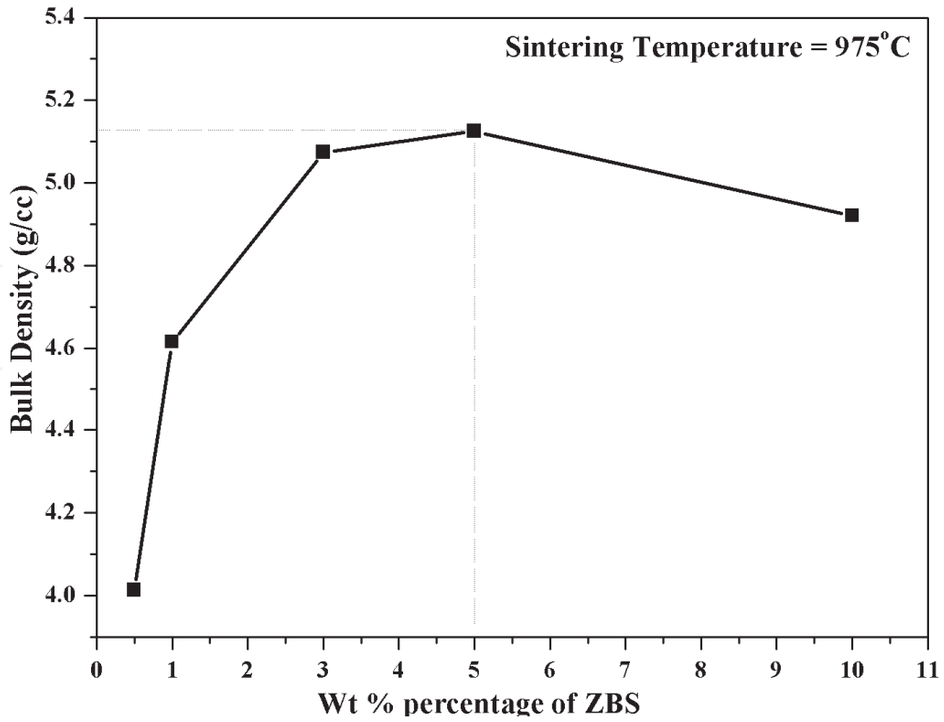

Fig. 7. Variation of bulk density of ZN ceramics (solid state synthesis) with different wt% of ZBS glass

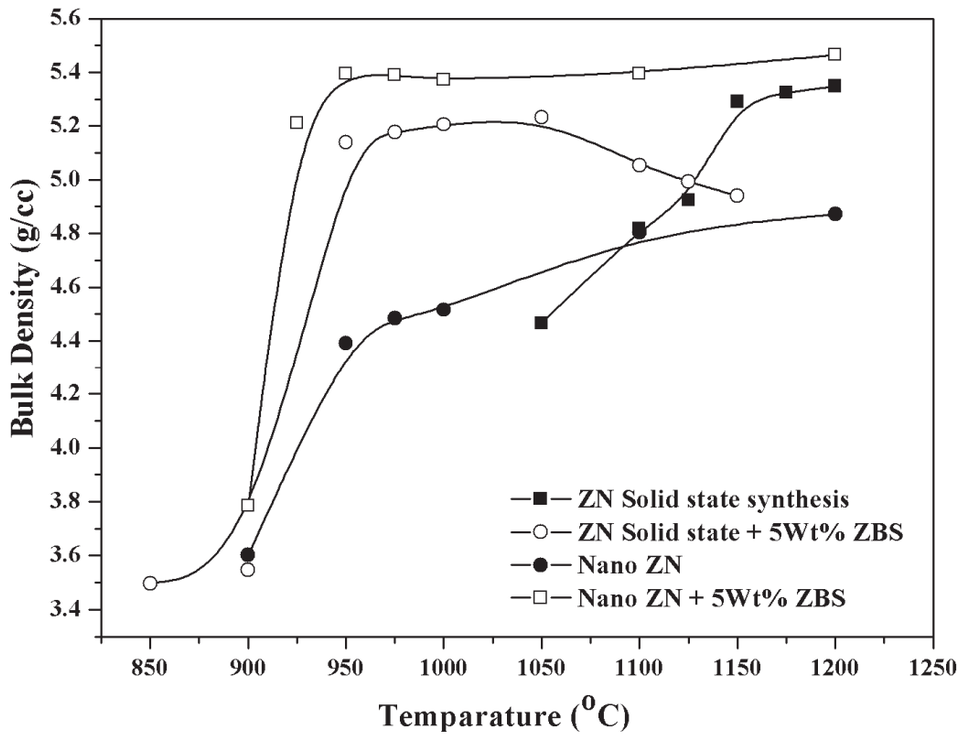

Fig. 8. Variation of the bulk density of ZN ceramics and ZN-glass composites with different temperature

nano sized ZN ceramics. In the case of glass addition, low melting glasses such as ZBS enhances the sinterability of the ZN ceramic powders due to the liquid phase sintering [25,26]. The glasses start melting at lower temperatures and the molten glasses flows through the porosity between the grains and fill the porosity and the gap between the grain Boundaries [27]. This enhances the sinterability *i.e.* the composite gets densified at lower sintering temperatures. Hence the ZN composite with 5 wt% ZBS glass shows higher density than that of the pure materials. The effect of liquid phase sintering is clearly seen in the SEM micrographs (Fig. 9) as molten glass melted at low temperatures.

Fig 9 shows the SEM micrographs of the sintered ZN. Fig 9 (a) and (b) are SEM micrographs of ZN synthesised using solid state ceramic route. Large grains having average grain diameter of ~4.2 μm were observed for pure ZN. Though the sintering has taken place,

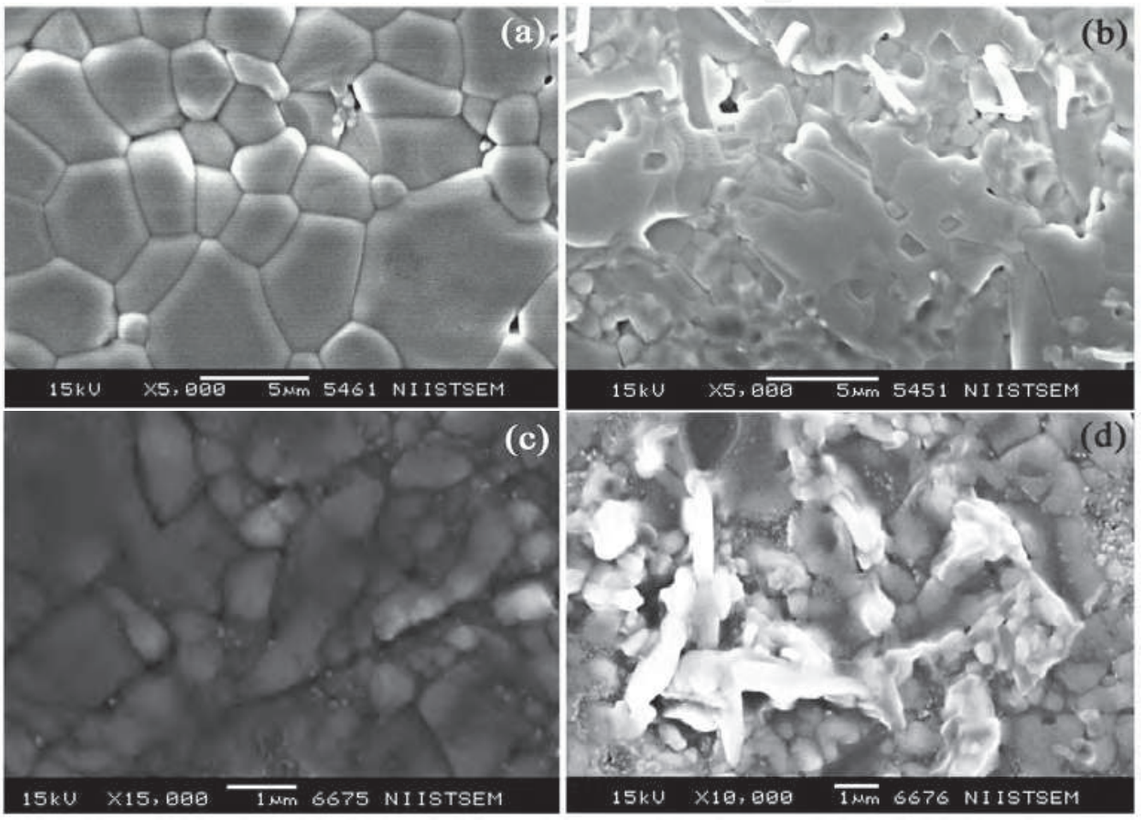

Fig. 9. SEM micrograph images of ZN ceramics and ZN-glass composites

Fig. 9 (b) shows a highly densified microstructure with large amount of molten glass phases for glass-ZN composites. It is observed that by the addition of ZBS glass the grain growth decreases. In fig 9 (b) the grains have an average diameter of about 1 to 2 μm only. Fig 9 (c) shows the SEM images of the sintered nano structured ZN (obtained via chemical synthesis) which are sintered at 925 ^{o}C for 2h. The SEM micrograph exhibits highly dense grains. Average grain size obtained from the micrograph images ranging from about 1-2 μm. It reveals fine sintered grains are obtained by sintering of nano ZN powder. Fig 9 (d) shows micro structure of the nanostructured ZN ceramic powders with 5wt% of ZBS glass. Comparatively smaller grains are obtained for the glass added nano powder compacts of ZN. The densification is very high for a much lower sintering temperature viz 925^{o}C/2hrs.

Comparing all images in Fig. 9 the nanostructured ZN with 5wt% of ZBS shows very high packing with a minimum porosity at 925 ^oC/2h.

The density and the dielectric properties viz dielectric constant ε_r, Qxf, and τ_f, of ZN ceramics are tabulated in table 2. Comparison of these properties of the materials synthesised by different preparation techniques reveals that the solid state synthesised shows greater values for dielectric constant and Qxf. This can be correlated with the effect of grain size. In ceramic materials the increase in the grain size deteriorates the dielectric loss. Reduction in the number of grains per unit volume, decreases of grain boundaries per unit volume and it would result in a material with a lower dielectric loss and better polarisability which improves both ε_r and Q×f [28,29]. From the SEM micrographs (Fig. 9) it can be concluded that the nanostructured ZN has more grain boundaries than solid state synthesised ZN and hence had a low ε_r and Q×f. However the glass addition to these compounds, due to liquid phase sintering the nanostructured ZN has greater densification at lower sintering temperature. The dielectric properties of micron sized ZN cermic with 5 wt% of ZBS are: density =5.48, ε_r = 21.3, τ_f = -66 ppm/^oC and with Q×f ~38,000, sintered at 975 ^oC/2h. Dielectric properties of sintered nano sized ZN with 5 wt% of ZBS have density = 5.21, ε_r = 22.5, τ_f = -69.6 ppm/^oC and with Q×f ~12,800, sintered at 925 ^oC/2h [30]. Since $ZnNb_2O_6$+5wt%ZBS can be identified as one of the potential LTCC materials sintering at 925^oC, co sintering studies were done with silver. $ZnNb_2O_6$+5wt%ZBS was mixed with 20wt% metallic Ag (99.99%) and sintered at 930^oC/2h. SEM pictures with EDAX was recorded after sintering and found that Ag is not reacting or melting during the sintering. Hence the co sintering of $ZnNb_2O_6$+5wt%ZBS+20wt%Ag was successful as can be seen in fig.10.

hkl Plane	d spacing from TEM (Å)	d spacing from ICDD file(Å)
111/310	3.6494	3.3602
311	2.9559	2.8455
020	2.8630	2.6789
002	2.5200	2.3098
312	2.0736	1.9918
131/330	1.7703	1.5676
313	1.5260	1.3099
041	1.3770	1.1561

Table 1. d spacing of major reflecting planes determined from TEM analysis

Materials	Sintering temperature (^oC)	Density (ρ) (g/cc)	ε_r	Qxf (GHz)	τ_f (ppm/^{o}C)
$ZnNb_2O_6$ – solid state synthesis	1200	5.32	23.3	12,800	-77.9
$ZnNb_2O_6$ + 5wt% ZBS	975	5.48	21.3	38,000	-66.0
$ZnNb_2O_6$ – polymer complex synthesis	1200	4.87	19.2	77,900	-66.4
$ZnNb_2O_6$ + 5wt% ZBS	925	5.21	22.5	12,800	-69.6

Table 2. Density and microwave dielectric properties of ZN and ZN-glass composites

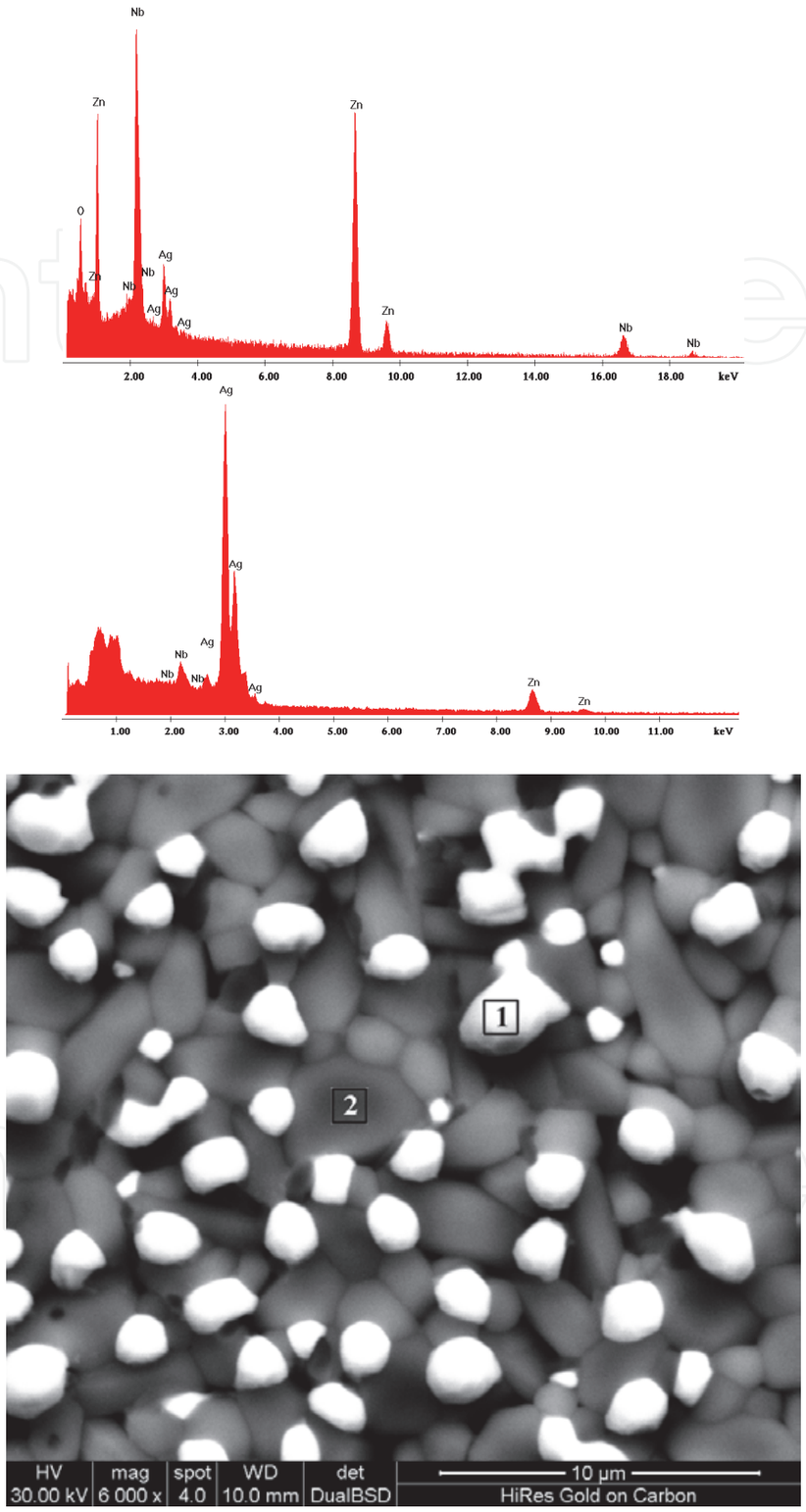

Fig. 10. SEM with EDAX micrographs of $ZnNb_2O_6$+5wt%ZBS+20wt% metallic Ag-Sintered at 930°C/2h

4. Conclusions

Zinc Niobates ceramics were prepared in phase pure powder form using solid state ceramic technique and polymer complex method. Particle size of the ZN ceramics is determined using TEM and it is found most of the particles are in the range 18-20 nm, the particle size obtained from XRD pattern using Debye Sherrer formula is 17 nm. Effect of particle size on the sinterability and the microwave dielectric properties were studied. Micro structure shows that a high density ZN ceramics can be obtained by sintering nanopowder of ZN with 5wt% of ZBS glass at 925 ^oC for 2h. Optimized sintering of nano sized powder at 925 ^oC/2h give microwave dielectric properties of ε_r =22.5, Qxf~12,800 and τ_f= -69.6 ppm/^oC. These composites were successfully co sintered with silver.

5. References

The influence of $ZnNb_2O_6$ on the microwave dielectric properties of $ZrTi_2O_6$ ceramics,Parinaz RiaziKhoei, Feridoon Azough, Robert Freer, J.Am. Ceram. Soc. 89[1] 216-223 (2006).

Characterization and Microwave Dielectric Properties of $M^{2+}Nb_2O_6$ Ceramics, Robert C. Pullar, Jonathan D. Breeze, Neil McN. Alford, J. Am. Ceram. Soc., 88 [9] 2466–2471 (2005)

Influence of Copper(II) Oxide Additions to Zinc Niobate Microwave Ceramics on Sintering Temperature and Dielectric Properties, Dong-Wan Kim, Kyung Hyun Ko, Kug Sun Hong, *J. Am. Ceram. Soc.*, 84 [6] 1286–90 (2001).

Low sintering ceramic materials based on Bi_2O_3-ZnO-Nb_2O_5 compounds, E. A Nenasheva, N.F Kartenko, J. Eur. Ceram. Soc 26, 1929-1932 (2006)

Low temperature sintered $ZnNb_2O_6$ microwave dielectric ceramics doped with ZnO-V_2O_5 additions, Jin Wang, Zhenxing Yue, Zhilun Gui, Longtu Li, J. Mater. Sci. 40, 6581-6583 (2005)

Synthesis and Microwave dielectric properties of $Zn_{1+x}Nb_2O_{6+x}$, A.G Belous, O. V Ovchar, A. V Kramarenko, B. Jancar, J Bezjak, D. Surnov, Inorg. Mater. 43, [3] 227-280, (2007).

Synthesis, characterization and microwave dielectric properties of $ATiO_3$ (A=Co, Mn, Ni) ceramics. P.S. Anjana and M T Sebastian. J. Am. Ceram. Soc. 89 (2006) 2114-2117.

Effects of $ZnCl_2$ addition on the $ZnNb_2O_6$ powder synthesis through molten salt method, Guo Liangzhai. Dai Jinhui, Tian Jintao, Zhu Zhibin, He Tian, Qu Xiaofei, Liu Zhongfang, Mater. Chem. and Phys. 105, 148-150 (2007).

H. Jantunen, R. Rautioaho, A. Uusimaki, S. Leppavuori, J. Eur. Ceram. Soc., 20 (2000), 2331-36.

M. T. Sebastian, H. Jantunen, Int. Mater. Rev., 53, (2008), 57-90.

M Laren, C. B. Ponton, J. Mater. Sci., 33 (1998), 17-22.

O. Renoult, J. P.Boilot, F. Chaput, R. Papiernik, L. G. Hubert-Pfalzgraf, M. Lejeune, J. Am. Ceram. Soc. 75 [12] (1992), 3337-40.

C. L. Huang, C. L. Pan, J. Mater. Sci. Lett. 21, (2002), 149-151.

H. Jantunen, R Rautioho, A. Uusimäki, S. Leppävuori, J. Eu. Ceram. Soc. 20 (2000), 2331-2336.

Synthesis of rare-earth orthoaluminates by a polymer complex method, Hirofumi Takata, Misako Iiduka, Yoshihiko Notsu, Masaaki Harada, J.Allys. Compd. 408-412,p 1190-1192 (2006).

Direct chemical synthesis of high coercivity air-stable SmCo nanoblades, C.N. Chinnasamy, J.Y. Huang, L.H. Lewis, B. Latha, C.Vittoria, V. G. Harris, Appl. Phys. Letts. 93, 032505 (2008).

Low temperature powder synthesis of $LaAlO_3$ through *in situ* polymerization route utilizing citric acid and ethylene glycol, Masato Kakihana, Toru Okubo, J. Allys. Compds. 266 (1998) 129–133.

Nanocrystalline materials and coatings, S.C. Tjong, Haydn Chen, Mater. Sci. Engg. R 45 (2004) pp 1-88.

Sintering and Characterization of Nanophase Zinc Oxide, Anne P. Hynes, Robert H. Doremus, Richard W. Siegel, J. Am. Ceram. Soc. 85[8] (2002) 1979-87.

C. L Huang, M. H Weng, Mater. Res. Bull. 36 (2001) 2741–2750.

C. L. Huang, J. L. Hou, C. L. Pan, C. Y. Huang, C.W. Peng, C. H. Wei, Y. H. Huang, J. Alloys Comp. 450 (2008) 359–363.

C. L Huang, C. H. Shen, C. L Pan, Mater. Sci. Eng. B 145 (2007) 91–96.

Sinterability studies and microwave dielectric properties of sol–gel synthesized $Ba(Zn_{1/3}Ta_{2/3})O_3$ nanoparticles, Manoj Raama Varma, P. Nisha and P.C. Rajath Varma, Journal of Alloys and Compounds, 457, 2008,422-428

Progress on grain growth dynamics in sintering of nano-powders, LIU Chunjing , Wang Xin , Jiang Yanfei , Wang Yongming , Hao Shunli, Rare Metal, Vol. 25, Spec. Issue , Oct 2006, P .471

V. K. Singh, J. Am. Ceram. Soc. 64 (1981) C 133-135.

J. H. Jean, S. C. Lin, J. Mater. Res. 14 (1999) 1359-1363.

Forsterite-based ceramic–glass composites for substrate applications in microwave and millimeter wave communications, T.S. Sasikala, M.N. Suma, P. Mohanan, C. Pavithran, M. T. Sebastian, J. Alloys Comp. 461 (2008) 555–559.

Microwave dielectric loss of titanium oxide, Alan Templeton, Xiaoru Wang, Stuart J. Penn, Stephen J. Webb, Lesley F. Cohen and Neil. McN. Alford, J.Am Ceram Soc. 83 (1) 95-100 (2000).

Effect of porosity and grain size on the Microwave Dielectric properties of Sintered Alumina, Stuart J Penn, Neil McN. Alford, Templeton, Xiaoru Wang, Meishing Xu, Michael Reece, and Kelvin Schrapel. J.Am Ceram Soc. 80(7) 1885088(1997)

Finite size effect on Sinterability and Dielectric Properties of $ZnNb_2O_6$ – Glass Composites, Mukkuttiparambil Ayyappan Sanoj, Chalappurath Pattelath Reshmi and Manoj Raama Varma, J. Am. Ceram. Soc. 92(11):2648-2653;Nov 2009

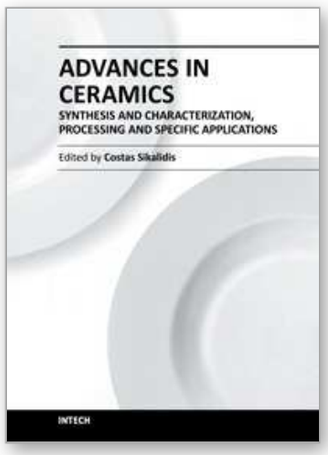

Advances in Ceramics - Synthesis and Characterization, Processing and Specific Applications

Edited by Prof. Costas Sikalidis

ISBN 978-953-307-505-1
Hard cover, 520 pages
Publisher InTech
Published online 09, August, 2011
Published in print edition August, 2011

The current book contains twenty-two chapters and is divided into three sections. Section I consists of nine chapters which discuss synthesis through innovative as well as modified conventional techniques of certain advanced ceramics (e.g. target materials, high strength porous ceramics, optical and thermo-luminescent ceramics, ceramic powders and fibers) and their characterization using a combination of well known and advanced techniques. Section II is also composed of nine chapters, which are dealing with the aqueous processing of nitride ceramics, the shape and size optimization of ceramic components through design methodologies and manufacturing technologies, the sinterability and properties of ZnNb oxide ceramics, the grinding optimization, the redox behaviour of ceria based and related materials, the alloy reinforcement by ceramic particles addition, the sintering study through dihedral surface angle using AFM and the surface modification and properties induced by a laser beam in pressings of ceramic powders. Section III includes four chapters which are dealing with the deposition of ceramic powders for oxide fuel cells preparation, the perovskite type ceramics for solid fuel cells, the ceramics for laser applications and fabrication and the characterization and modeling of protonic ceramics.

InTech Europe
University Campus STeP Ri
Slavka Krautzeka 83/A
51000 Rijeka, Croatia
Phone: +385 (51) 770 447
Fax: +385 (51) 686 166
www.intechopen.com

InTech China
Unit 405, Office Block, Hotel Equatorial Shanghai
No.65, Yan An Road (West), Shanghai, 200040, China
中国上海市延安西路65号上海国际贵都大饭店办公楼405单元
Phone: +86-21-62489820
Fax: +86-21-62489821

IntechOpen